LA-UR-99-? -5992

Title: Groundwater Flow and Radionuclide Transport Calculations for a Performance Assessment of a Low-Level Waste Site

Author(s): Kay H. Birdsell*, Los Alamos National Laboratory
Andrew V. Wolfsberg, Los Alamos National Laboratory
Kathleen M. Bower, Eastern Illinois University

*Contact for correspondence

Submitted to: The Journal of Contaminant Hydrology

Los Alamos
NATIONAL LABORATORY

ABSTRACT

A method for performing radionuclide transport analyses to support performance assessment of low-level radioactive waste sites is developed and applied to a site at Los Alamos National Laboratory. The analyses predict the fate of the waste from its source, through the vadose zone, into the saturated zone, and finally, its potential dose at the accessible environment. The calculations are run with the finite-element code FEHM, which simulates fluid flow, heat transport, and contaminant reactive transport through porous and fractured media.

The modeling approach for this study couples realistic source-term models with an unsaturated-zone flow and transport model, which is then linked to the saturated-zone flow and transport model. The three-dimensional unsaturated-zone flow and transport model describes the complex hydrology associated with the mesa-top and volcanic geology of the site. The continued migration of nuclides into the main aquifer is calculated using a three-dimensional, steady-flow, saturated-zone model that maintains the spatial and temporal distribution of nuclide flux from the vadose zone. Preliminary results for the aquifer-related dose assessments are made, and these doses are well below relevant performance objectives for low-level waste sites. A general screening technique that can greatly reduce the number of contaminants requiring full analysis in a site assessment is also presented.

Keywords: Performance Assessment, Hydrology, Radioactive Waste, Unsaturated Zone

INTRODUCTION

Environmental concerns associated with radionuclides in groundwater are a legacy of nuclear energy and nuclear weapons development over the last fifty years. Risk analyses and performance assessments for radioactive waste disposal sites rely heavily on transport calculations that predict the migration of radionuclides through the subsurface over thousands of years. This paper presents a method for predicting the performance of a low-level radioactive waste site through a case study of the active, low-level radioactive waste site located at Los Alamos National Laboratory (LANL) in northern New Mexico, as shown in Figure 1.

Whereas performance assessment models do not generally incorporate explicitly the detailed processes and site-characterization data (e.g., Wilson et al., 1994), our method uses process models to calculate the source release of the waste, the continued migration of the waste through the unsaturated and saturated zones, and finally, the potential aquifer-related doses. We also present general screening and scaling techniques that help to make site assessment with process-level models manageable by reducing the number of contaminants requiring full analyses. Thus, providing a tractable method for using detailed process modeling on a performance assessment.

The three-dimensional unsaturated-zone flow and transport model captures the complex hydrogeology and topography of the site and yields radionuclide flux estimates to the regional aquifer. Within the unsaturated-zone model, the source release of radionuclides is computed for thirty-eight waste disposal pits and four shaft fields, each contributing to the total inventory. The continued migration of radionuclides through the aquifer is calculated using a three-dimensional model designed to maintain the temporally and spatially varying distribution of radionuclide flux from the unsaturated zone. Finally, groundwater concentrations are converted to aquifer-related doses for risk analysis. All calculations were run with the finite-element code FEHM (Zyvoloski et al., 1997) which simulates single- and multi-phase fluid flow and reactive contaminant transport through porous and fractured media.

SITE DESCRIPTION

STRATIGRAPHY AND TOPOGRAPHY

The strata that lie beneath LANL are composed of a series of nonwelded to moderately welded rhyolitic ash-flow and ash-fall tuffs underlain by a thin pumice bed, a thick basalt, and a conglomerate formation (Krier, et al., 1997) as shown in Figure 2. The tuff layers were deposited during violent eruptions of volcanic ash from the Valles caldera some 1.2 to 1.6 million years ago (Rogers and Gallaher, 1995). Since then, the tuff has eroded to leave a system of alternating finger mesas and canyons. LANL's low-level waste (LLW) disposal facility is located atop one such mesa with the waste buried in disposal pits and shafts to a depth of approximately 20 meters. The

surrounding canyons lie 30 m below the steep-sided mesa, and the water table is located approximately 250 to 300 meters below the disposal pits.

The upper six stratigraphic units make up the Bandelier Tuff. These units both dip gently and thin toward the eastern end of the site. The top two tuff layers, Unit 2 and Unit 1v-u, are extensively fractured and are separated by a thin interval called a surge bed (Krier et al., 1997). The surge bed is made up of fine, sand-sized material and is genetically related to the main deposits of poorly sorted, relatively massive ashflow tuff (Fisher, 1979). The deeper tuff units have little observed fracturing (Krier et al., 1997).

The Cerros del Rio Basalts, which comprise over 50% of the unsaturated zone, display wide variability (Turin, 1995), ranging from extremely dense with no apparent porosity, to highly fractured, to so vesicular as to appear foamy. The fanglomerate member of the Puye Conglomerate lies at the base of the unsaturated zone and extends into the saturated zone. The fanglomerate consists of volcanic debris such as cobbles and boulders in a matrix of silts, clays, and sands (Purtymun, 1995). Clay, silt and pumice lenses, and interbedded basalts are also common

CONTAMINANT SOURCE

The waste disposal facility occupies about 300,000 m^2 atop a finger mesa with waste buried in pits and shafts to a depth of approximately 20 m. In the pits, the waste is layered and compacted to improve stability, and void spaces are backfilled with crushed tuff to minimize subsidence. A typical pit contains at least 60 percent consolidated crushed tuff (Hollis et al., 1997). Between 1957 and 1995, radioactive waste was buried in 34 disposal pits and in almost 200 shafts located in five shaft fields. The waste form buried at the site contains over sixty radionuclides with the majority of the waste being ^{235}U, ^{238}U, and ^{232}Th. Currently, only low-level radioactive waste is accepted, but prior to 1971, transuranic and mixed waste were also accepted (Shuman, 1997a). An expansion area with four large pits and another shaft field is planned for operation through 2044 and is included in this study.

The oldest wastes are buried at the eastern-most portion of the site, and disposal operations have proceeded toward the west (see Figure 3). The waste is categorized in terms of four disposal-unit classifications that are determined by the age of the wastes because wastes disposed during different time periods are governed by different regulations and because inventory records have improved with time. Whereas the performance assessment (PA) evaluates the releases for the 1988-1995 and projected 1996-2044 wastes, the composite analysis (CA) evaluates releases from all wastes, past and future. However, detailed inventory data are not available prior to 1971 and are uncertain for future activities. Therefore, the inventory in the 1957-1970 waste is extrapolated backwards based on disposal operations from 1971 to 1977, and the inventory for the 1996-2044

waste is projected based on current operations and expected future operations. The inventories for the 1971-1988 waste and the 1988-1995 waste are obtained from disposal records. The inventory information required to model the source release for each nuclide from a particular disposal pit or shaft field include the total nuclide inventory, the appropriate source-release model, the initial nuclide waste volume, and the solubility limit. This information was obtained from Shuman (1997a) and Vold and Shuman (1996).

HYDROLOGIC DATA

The van Genuchten model (van Genuchten, 1980) is used to represent the moisture retention characteristic curves for all units in the unsaturated zone model. The parameters for this model (saturated permeability, porosity, inverse air entry pressure, etc.) are fairly well characterized for the six Bandelier Tuff units and for the crushed tuff used as pit backfill but not for the deeper units. The properties for the tuff units (Krier et al., 1997), the crushed tuff, and the Guaje Pumice were measured on core samples of matrix material. Estimated values for the saturated conductivity and porosity of the Puye Conglomerate (Purtymun, 1984) are used, and we assume that the van Genuchten fitting parameters are similar to those of a coarse sand. No hydrologic property data were available for the basalts at the time this study was performed. Therefore, the basalt matrix properties of a vesicular basalt located beneath Idaho National Engineering Laboratory are used as an analog (Bishop, 1991). Table 1 summarizes the hydrologic parameters used for all of the units in the unsaturated zone flow and transport model.

The upper two tuff units are fractured and extremely dry as demonstrated by the site data in Figure 4. Much of the data collected at the site indicate evaporation within the mesa top including low mesa-top saturation values (Krier et al., 1997), chloride and $\delta^{18}O$ profile analyses (Newman, 1996), and high matrix potential measured along the surge bed (Rogers et al., 1995). For example, high porewater chloride concentrations observed in the mesa lead to flux estimates ranging from 0.03 to 1.5 mm/yr while chloride concentrations below the canyon level yield fluxes near 5 mm/yr (Newman, 1996). Previous numerical simulations indicate that evaporative effects can reasonably account for the low moisture contents observed in undisturbed regions of the mesa at the site and can justify a low net percolation rate (Birdsell et al., 1997).

TRANSPORT PROPERTIES

Site-specific Kd values were measured for Am, Np, Pu, Tc, and U on local samples for intact unsaturated tuff, crushed tuff, and intact saturated tuff (Longmire et al., 1996). Kd values for the remaining nuclides in the inventory are based on sorption measurements for Yucca Mountain tuffs (Krier et al., 1997). The Kd values for all nuclides considered in this study are shown in Table 2.

Site-specific values for diffusion coefficients and dispersivity are not available. We therefore estimate values of these parameters. Recent studies by Conca (1992) show that the diffusion coefficient decreases as saturation decreases. For the unsaturated zone, the diffusion coefficient is modeled in this fashion and decreases parabolically from 10^{-9} m^2/s at saturation to 10^{-15} m^2/s at a moisture content of 0.001. For the saturated zone, the diffusion coefficient is assumed to be 10^{-9} m^2/s, consistent with the unsaturated-zone model at full saturation.

In the unsaturated zone, the dispersivity used is 1 m in the vertical direction and 0.1 m in the horizontal plane. Larger dispersivity values of 20 m in the direction of flow and 2 m transverse to the flow are used for the saturated zone because field studies have shown that dispersivity in the saturated zone increases with scale (Neuman, 1990; Gelhar et al., 1992). These are estimated using an empirical fit to field data developed by Neuman (1990) based on a length scale of approximately 100 m, the distance from the site boundary to the compliance point.

CONCEPTUAL MODEL

The conceptual model on which the numerical simulations are based includes spatially variable infiltration, mobilization and release of radionuclides from the pits and shafts, migration of radionuclides through the unsaturated, fractured tuff, and finally transport in the saturated zone.

Infiltration

The average precipitation rate for the area is 35.6 cm/yr (Bowen, 1990). Most of this precipitation is lost to runoff and evapotranspiration, resulting in a heterogeneous infiltration pattern that is controlled by the mesa/canyon setting of the site. Infiltration is thought to be seasonal with most occurring during spring snowmelt and, to a lesser extent during, the summer thunderstorm season (Rogers et al., 1997). Figure 2 shows the different regions in which infiltration occurs. Based on measured rock saturations and chloride data, a very low net percolation rate (1 to 10 mm/yr) is thought to exist within the mesa. Pajarito Canyon is wetter with an estimated percolation rate of 10 to 100 mm/yr, while Cañada del Buey is dry with a percolation rate similar to the mesa top. The steep mesa sides represent an evaporative region (water sink) rather than a source region. The coupling of the fractured units separated by the high-permeability surge bed with the mesas topographic relief is thought to enhance air circulation and consequently evaporative drying within the mesa interior. However, pit excavation through the upper two units destroys both the fracture network and the continuity of the surge bed, which likely disrupts the mesa's natural capacity for subsurface evaporation. In designing the boundary conditions for the predictive models, preliminary simulations investigate how well modeled and observed saturations correspond for various infiltration rates, how appropriate a steady-state infiltration rate is, and the representation of fracture matrix interactions. These are described in the numerical modeling section of this paper.

Release of Radionuclides

The release of radionuclides from the disposal units is represented by one of two release mechanisms, rapid release and solubility limited. The maximum pore-water concentration of each nuclide is compared to its solubility limit to determine which source-release model is appropriate for each nuclide in each disposal unit. That is, if the maximum pore-water concentration exceeds the nuclide's solubility limit, the release concentration is held at the solubility limit until that nuclide's inventory has been exhausted. The contaminant flux (Φ) for the solubility-limited model takes the form

$$\Phi = f_{ij} V q C_{sl} / h ,$$

where V is the total initial nuclide waste volume in the disposal unit, q is the Darcy flux through the waste package, C_{sl} is the nuclide solubility limit, and h is the representative height of a waste package (taken to be 1 m). The fraction f_{ij} is a correction factor for the solubility limit contributions from multiple nuclides, i, of the same element and from multiple waste forms, j. This correction factor was determined to be a significant only for uranium, which is solubility limited throughout the site (Vold and Shuman, 1996). Wastes may be solubility limited in some disposal units and rapid release in others, depending on the inventory and volume in the particular disposal unit. For example, much larger quantities of plutonium are disposed of in smaller-volume shafts than in larger-volume pits. As a result, the release of plutonium is solubility limited from the shafts but not the pits.

If the pore-water concentration does not exceed the nuclide's solubility limit, the rapid-release model is used. Nuclides with very large solubility limits, such as ^{129}I and ^{99}Tc, are controlled by this mechanism throughout the site. The contaminant flux for the rapid-release model takes the form

$$\Phi = Q \lambda 2te^{-\lambda t} ,$$

where Q is the total inventory (moles) of the nuclide in the disposal unit and λ is the release constant ($\lambda = q/\theta h$), and θ is the average moisture content of the disposal unit (taken to be 0.08). The rapid-release source term is highly dependent on the Darcy flux through the waste package (q), which is assumed to equal the percolation rate (see Figure 5). For example, with a percolation rate of 10 mm/yr, the rapid-release model predicts that the waste is completely released within the first 80 years, while at a percolation rate of 1 mm/yr, release from the waste package requires more than 500 years.

Unsaturated-Zone Transport Processes

The fundamental processes affecting migration rates of solutes in this unsaturated environment are advection, adsorption, diffusion, dispersion, and radioactive decay. A linear adsorption isotherm (Kd model) is expected to adequately describe adsorption in the unsaturated zone because of the slow percolation rates and the indication that transport occurs predominantly in the matrix in the units above the basalt. Once released from the disposal unit, the mesa-top infiltration rate, its Kd, and its half-life control the mobility of a nuclide through the unsaturated zone. Thus, the nuclides can be classified by their half-lives and adsorption characteristics. Short-lived nuclides with half-lives less than 20 years, such as ^{3}H and ^{60}Co, are expected to decay to insignificant levels before reaching the aquifer, so they are not considered in the analysis. Sorption characteristics of nuclides lead to nonsorbing, weakly sorbing, and strongly sorbing groups, as shown in Table 2. The nonsorbing nuclides ^{14}C, ^{129}I, and ^{99}Tc are expected to travel most rapidly, while the strongly sorbing nuclides are expected to have very long travel times.

Since we cannot predict whether transport is controlled by matrix or fracture flow processes in the basalt, we conservatively treat the basalts as a system dominated by vertical fracture flow. This is done by modeling the basalt as an equivalent continuum medium made up of both fractures and matrix material (Klavetter and Peters, 1986). Matrix properties are derived from the analogue basalts in Idaho. Fracture properties are chosen such that no lateral diversion occurs at the top of the basalts, even when the flow exceeds the matrix saturated hydraulic conductivity. Then, since it is not known under which conditions fracture flow actually initiates, matrix and fracture porosity are set equal to the fracture volume fraction, 10^{-4}, to insure rapid transport of one to five years through this unit, hence forgoing any retardation due to matrix flow or sorption. This treatment of transport through the basalt yields a conservative PA result (e.g., faster groundwater travel times and higher peak doses than actually expected). The basalts are also assumed to be nonsorbing, consistent with the assumption of rapid transport through this unit.

Saturated-Zone Flow and Transport Processes

Groundwater that percolates from the site through the unsaturated zone is assumed to flow predominantly downward to the main aquifer. Any radionuclides exiting the base of the unsaturated zone enter the saturated zone through the upper boundary. Although an understanding of the geology and groundwater system under LANL is still being developed, Purtymun (1995) suggests that the groundwater in the main aquifer flows in a southeasterly direction to the Rio Grande. Our saturated-zone model is based on this hypothesis. Advection, linear adsorption, diffusion, dispersion, and radioactive decay again control saturated-zone migration of solutes.

NUMERICAL MODEL

OVERVIEW

The unsaturated-zone model is a three-dimensional representation of the complex mesa/canyon hydrogeologic system. Infiltration is assumed to be steady in time but variable in space over the mesa top and two bordering canyons. The model incorporates the position and inventories of thirty-four disposal pits and five shaft fields already located at the site along with those of the proposed expansion pits and shafts. Two pathways are considered: downward migration through the unsaturated zone to the aquifer, and lateral migration to the mesa sides followed by deposition into the nearby canyons, and subsequent migration through the unsaturated zone to the aquifer. Time- and spatially-variable nuclide flux from the unsaturated zone enters the single material, three dimensional, saturated-zone model, maintaining the spatial distribution of nuclide flux exiting the unsaturated zone. The simulations are run for 10,000 years to cover the regulatory-driven 1000-year compliance period (Hollis et al., 1997) with a 10,000-year uncertainty analysis.

The simulations are run with FEHM, a two- or three-dimensional finite-element/finite-volume code suitable for simulating systems with complex geometries that arise when modeling subsurface flow and transport (Zyvoloski et al., 1997). In the unsaturated zone, the governing equations for flow are based on the principles of conservation of water and air. Darcy's law is assumed to be valid for the momentum of the air and water phases in the unsaturated zone and for the water phase in the saturated zone. The convection-dispersion equation governs solute transport (Zyvoloski et al., 1997; Jury et al., 1991) in these analyses.

COMPUTATIONAL GRID

The stratigraphic configuration used for the unsaturated-zone model is derived from various sources including the LANL site-wide geologic model (Vaniman et al., 1996), well-log picks, and surface observations. The data set is interpolated with the Stratagraphic Geocellular Modeling (SGM) Software (Stratamodel, Inc., Copyright 1994) to generate the three-dimensional geologic framework model shown in Figure 6, which includes the thinning of the Bandelier tuff units at the eastern end of the site.The three-dimensional unsaturated-zone grid is generated with the Geomesh/X3D software (Gable et. al, 1995) from the geologic framework model. An initial grid is constructed with the 45.7-m spacing of the geologic framework model and then resolved to include the 38 waste disposal pits (Fig. 3) and to better delineate the mesa sides. The final grid contains 41,542 nodes and 254,614 tetrahedral elements. Pit regions are defined by a set of nodes that outline several adjacent pits with internal nodes down the pit centerlines that have volumes that approximate true pit volumes. The internal pit nodes are assigned hydrologic properties for crushed tuff (the pit backfill material) and act as the source region for radioactive waste during the transport calculations. Figure 3 shows the outline of the waste disposal pits, the internal pit nodes, and the outline of the mesa edge.

The saturated-zone model extends from just west of the site to the Rio Grande. The grid is rectangular shaped and oriented perpendicular to groundwater equipotentials. It is 9,773 m long 1,280 m wide, and 100 m deep with 19,580 nodes and 102,960 tetrahedral elements. To better model the vertical dispersion of the contaminant plumes entering the aquifer from the unsaturated zone, the vertical element height is refined near the water table. The grid is also refined horizontally beneath the site to approximately 500 m downstream in order to accurately capture the spatial distribution of the radionuclides as they move toward the downstream compliance regions.

BOUNDARY CONDITIONS

Preliminary Calculations

As described in the conceptual model, a series of preliminary calculations were performed to evaluate infiltration rates and modeling assumptions, such as the use of steady flow rates and the dominance of matrix flow through the tuff units.

To determine appropriate infiltration rates for the site, simulated saturation profiles for a number of different steady, mesa-top infiltration rates (10 mm/yr, 1 mm/yr, 0.1 mm/yr, 0.01 mm/yr and 0.0 mm/yr) using the two-dimensional cross section shown in Figure 2 are compared to site field data. Figure 4 shows calculated steady-state saturation profiles at the center of the mesa for the five infiltration rates along with the ranges of in-situ saturation data measured in the six Bandelier Tuff units. The shape of the calculated saturation profiles shows the same trend as the data (e.g. saturations decrease from Unit 2 to Unit 1v-u and then increase again in Unit 1v-c, etc.), but no single infiltration rate yields predicted saturation values that fit the entire data set. Results for the lowest infiltration rates (0.01 and 0.0 mm/yr) most closely match the site saturation data in Units 2 and 1v-u, the two mesa-top units. Higher infiltration rates (1 and 0.1 mm/yr) are needed to match the saturation data from Units 1v-c and 1g, and an even higher rate (10 mm/yr) is needed to match the data in the Cerro Toledo and the Otowi Member. Newman (1996) also found that no single percolation rate fits insitu chloride data gathered at the site. For example, he estimates midmesa flux rates ranging from 0.03 to 1.5 mm/yr and submesa flux rates near 5 mm/yr based on chloride flux estimates. Based on these two studies, the PA calculations use a range of mesa-top infiltration rates from 1 to 10 mm/yr.

Since deep percolation is thought to be seasonal with most occurring during spring snow melt and to a lesser extent during the summer thunderstorm season (Rogers et al., 1997), separate, small-scale modeling studies were performed to test the assumption of steady-state flow used for the performance assessment calculations. Birdsell et al. (1997) studied the effects of annual transients in percolation rate on unsaturated-zone transport at the site and found that simulated transient pulses are damped with depth so that the calculated cumulative contaminant flux at the base of the Bandelier Tuff is similar under transient and steady flow fields. By using a steady infiltration rate

at the high end of the expected range, and forcing short travel times through the basalt, the subsequent transport calculations are expected to yield conservative results, assuming that fracture flow has little effect on transport in the upper two fractured tuff units.

Numerical studies of fracture flow for the site (Soll and Birdsell, 1997) indicate that transport through fractured tuffs has a minimal effect on contaminant flux at depth. Also, during pit emplacement the uppermost unit, Unit 2, and often part of Unit 1v-u are excavated, thus destroying the natural fractures in the area surrounding the waste. Because of these factors, fractures are only included for the deep basalt in the unsaturated-zone model.

Performance Calculations

The mesa/canyon setting leads to a set of spatially-dependent surface boundary conditions categorized by position depending whether infiltration is applied to the mesa top, to the relatively wet Pajarito Canyon, or to the dry Cañada del Buey. Evaporative nodes along the mesa sides are held at a fixed saturation of 0.03, which is equivalent to an ambient relative humidity near 50%.

Five different unsaturated-zone flow fields are considered in order to study the sensitivity of the simulated results to infiltration rate. Three mesa-top flows are used (1 mm/yr, 5 mm/yr, and 10 mm/yr), two flow rates for Cañada del Buey are considered (1 mm/yr and 5 mm/yr), and three flow rates for Pajarito Canyon are used (20 mm/yr, 50 mm/yr and 100 mm/yr). Table 3 summarizes the five cases. The base case, 5_1_50, is thought to be conservative for the site based on Newman's (1996) chloride flux estimates and on the saturation profiles shown in Figure 4, which show that the range 1 mm/yr to 10 mm/yr fits the higher range of site moisture data. No-flow boundary conditions are applied to the sides of the unsaturated-zone grid. The bottom boundary represents the water table, where both water and radionuclides can exit.

A steady flow field is calculated for the saturated-zone model by assuming a pressure head difference of 101 m (Purtymun, 1995) applied across the east and west sides of the model. No-flow boundaries are used for the top, bottom, north and south sides. A water balance estimate shows that the volume of water entering the aquifer from the unsaturated zone at the site is negligible compared to the aquifer volume (Birdsell et al., 1997). Recharge is assumed to occur mainly to the west of the site, at higher elevations in the Jemez Mountains. Thus, water flowing from the unsaturated zone to the aquifer is not included.

Simulated time-dependent radionuclide flux exiting the base of the unsaturated zone is recorded at each time step and used as the radionuclide source term for the saturated zone. To supply an adequate spatial distribution, the bottom boundary of the unsaturated-zone grid is divided into 28 regions for which nuclide flux is reported. Then, nodes corresponding to these 28 regions are

defined as source regions for the saturated-zone model to retain the spatial distribution of plumes that have migrated from the original disposal units.

SOURCE TERM

The source-release models to calculate time-dependent nuclide release rate from each disposal unit (Vold and Shuman, 1996) are incorporated directly into FEHM (Zyvoloski et al., 1997) and include both rapid release and solubility-limited release. Because wastes from the four disposal-unit classes are governed by different regulations (Hollis et al., 1997), the transport of each waste class is simulated separately. Then, these simulations determine the impact of an individual waste class or can be combined by superposition to determine the impact of the total inventory. Also, by differentiating the impact of the individual waste classes, the calculations can help define waste acceptance criteria for future wastes or a part of the analysis can be updated if inventory corrections are required.

The extrapolated total inventories for the 1957-1970 and 1996-2044 wastes (Shuman, 1997a) represent estimated and projected values, respectively. Because the distribution of waste among the individual disposal units within these two waste classes is not characterized, their inventories are uniformly distributed between all of the pit or shaft nodes for the particular waste class. However, inventory and waste volume are known in greater detail for the 1971-1988 and for the 1988-1995 wastes. For each nuclide in these two waste classes, the total inventory and waste volume is available for each pit and shaft field and is therefore distributed appropriately between the finite-element model nodes at the source locations.

DOSE

The saturated-zone radionuclide concentrations are converted to two types of doses: the groundwater dose results from the direct ingestion of groundwater extracted from the regional aquifer and the groundwater component of the all-pathways dose results from ingestion of groundwater and of foodstuffs raised with contaminated water. The dose conversion factors shown in Table 4 are used to convert aquifer concentrations to nuclide-specific doses. These factors are a function of the nuclide half-life and the consumption rates of water, food and soils (Shuman, 1997b). The total dose is the sum of the nuclide-specific doses. Once the total dose is calculated for the entire aquifer, the maximum dose is reported along a compliance boundary 100-m downgradient from the site fence line (Figure 3) as required by DOE regulations (Hollis et al., 1998). The groundwater doses are not only reported by their pathway (e.g., groundwater vs. all pathways) but doses are also reported by their original waste classification (PA or CA) as described in the source term discussion.

RESULTS

UNSATURATED-ZONE TRANSPORT

Screening

Unsaturated-zone transport calculations were run for ^{14}C, ^{129}I, ^{237}Np, ^{99}Tc, and ^{238}U using the base-case, steady flow field, 5_1_50 (see Table 3). These nuclides were chosen because of their low distribution coefficients, ranging from zero to 2.43 for most of the unsaturated-zone units. Only ^{14}C, ^{129}I, and ^{99}Tc, the nonsorbing nuclides, show any breakthrough to either the water table or the mesa side over the 10,000-year time frame. Thus, we are able to eliminate the remaining nuclides from consideration in the dose assessment because their distribution coefficients are larger than those of ^{237}Np and ^{238}U, which did not break through. This screening includes the consideration of all daughter products in the radionuclide decay chains, all of which have Kd values larger than those of ^{237}Np and ^{238}U. Calculations of ^{237}Np and ^{238}U transport using the highest flow rates, 10_5_100, also indicate no breakthrough, thus showing that this screening technique applies for all flow fields considered in this study.

This screening technique does not consider colloid-facilitated radionuclide transport. Although colloid-facilitated transport has recently been implicated with trace amounts of plutonium in the saturated zone at the Underground Test Area of the Nevada Test Site (NTS) (Kersting et al., 1999), there are several key differences between the NTS and LANL systems. Unlike the NTS, where radionuclides are essentially emplaced in the fractured, saturated-zone flow path, the source at LANL is in the unsaturated zone where fracture flow in most units is expected to be negligible. Whereas mobile colloids are abundant in saturated systems (DeGueldre et al., 1997), they are less abundant and less likely to be mobile in matrix flow dominated unsaturated systems. Low mobile colloid concentration, filtration due to size exclusion in pores, and retardation at air-water interfaces reduce the likelihood of colloids playing a significant role in enhancing migration of otherwise immobile radionuclides in the LANL system.

The screening technique used above is dependent on the 10,000-year uncertainty period. We have also developed another more general screening technique that is independent of the compliance period (Birdsell et al., 1995). The technique compares the nuclide's half-life to its unsaturated-zone travel time. Generic breakthrough curves are calculated for various Kd values to estimate a functional form for the time of first arrival (estimated in our case as 0.1% of the peak concentration) versus Kd. In twenty half-lives a waste decays to 10^{-6} times its original inventory. Thus, if a nuclide's unsaturated-zone travel time is greater than twenty times its half-life, there is essentially no release to the aquifer, and the nuclide requires no further consideration unless it has long-lived daughters. This comparison provides a generic method to eliminate transport calculations for a site with no strict regulatory compliance period. In a previous study of the LANL site, over half the nuclides were eliminated from further consideration with this method

(Birdsell et al., 1995). This screening technique can also be extended to any waste that exponentially degrades, including biodegradable wastes.

Transport Calculations

Base-Case Flow Field

Figure 7 shows simulated ^{129}I plumes in the unsaturated zone for the four age-dependent waste classes (Fig. 3) after 1000 years using the base-case flow field. Although the infiltration rate at each source region is the same, 5 mm/yr, the four plumes are quite different due to both inventory variations and geologic differences. The inventory distribution in the disposal units is heterogeneous, leading to large variations in radionuclide flux from the disposal units to the unsaturated zone. For example, the 1971-1988 inventory dominates the total site release of ^{129}I to the aquifer at 1000 years. Also, the 1988-1995 shafts located near the southern edge of the mesa (left side of Fig. 7c) concentrate nearly 80% of the 1988-1995 ^{129}I inventory into a small area thus producing a predominant plume at the southern portion of the mesa, while the pits to the north and west produce the less concentrated plumes. The location of the basalt unit and the effect of the vertical, fracture-dominated flow through this unit on plume migration is readily visible in these figures. We see that once solutes reach the basalt, they migrate quickly through the unit. In the 1996-2044 waste scenario (Fig. 7d), only the plume's leading edge reaches the basalt after 1000 years because the Bandelier Tuff units are much thicker beneath this proposed expansion area.

Figure 8 shows the total time-dependent flux of ^{129}I from the unsaturated zone to the saturated zone for the four waste classes (Fig. 3) using the base-case, steady flow field. This figure also demonstrates the dominance of the larger 1971-1988 inventory on ^{129}I releases from the site. The release of this nuclide is controlled by the exponential, rapid-release model, which produces flux-versus-time curves that peak in less than 10,000 years.

For each of the nuclides and the four waste classes, the solute flux is increasing at 1000 years causing the compliance-period peak dose to occur at 1000 years. Figure 8 shows that during the 1000-year to 10,000-year uncertainty period, the four ^{129}I curves peak at different times. The other two nuclides also show a distribution for the occurrence of the peak solute flux. Because of these distributions in time, a formal dose calculation is required to predict when the peak dose for the uncertainty period occurs.

Other Flow Fields

To assess the effect of uncertainty in flow rate on transport results, we examine the transport of the 1988-1995 ^{129}I inventory using different flow fields and compare nuclide fluxes through the unsaturated zone. Figure 9 shows the total flux of ^{129}I for the five flow fields described in Table 3. By comparing the 1_1_20 case, the 5_1_20 case, and the 10_1_20 case, we see that increased

mesa percolation leads to faster breakthrough and increased solute flux through the unsaturated zone. This flow-rate dependency is compounded by the velocity-dependent rapid-release source term (Figure 5). The solute flux at 1000 years for the lowest flow case, 1_1_20, is five to seven orders of magnitude less than the other cases considered. This case is used to predict the lower-bound dose in the uncertainty analysis. By comparing the 5_1_20 case to the 5_1_50 case, we see that additional flow through Pajarito Canyon results in faster breakthrough and increased solute flux to the saturated zone. The 10_5_100 case represents the wettest case and yields the fastest breakthrough and highest flux to the saturated zone, and consequently, the highest dose over the first 1000 years. This case is used to estimate an upper-bound dose for the uncertainty analysis.

The first arrival (0.1% of peak) of ^{129}I at the water table varies significantly for the different flow scenarios, as shown in Figure 9. For the base-case calculations, the time of first arrival is about 600 years. Whereas the first arrival for the highest flow case is half the 600 years of the base case, the lowest flow case's first arrival is at 2000 years, well beyond the 1000-year compliance period.

Lateral Transport toward the Mesa Sides

Lateral flux of nuclides toward the mesa sides is observed in the simulations (see Fig. 7), so the impact of this pathway on the dose is assessed here. As in the case of downward transport, only the three nonsorbing nuclides ^{14}C, ^{129}I and ^{99}Tc are of concern over 10,000 years. To summarize, our analysis of this pathway takes several steps. First, the transport of nuclides through the unsaturated zone is simulated, yielding the nuclide flux to the two mesa sides. Next, we conservatively assume that the radionuclide flux through the mesa sides is immediately available for transport from either Pajarito Canyon or Cañada del Buey, where their continued migration to the aquifer is simulated. Those contaminants reaching Pajarito Canyon lead to the highest aquifer-related doses because of the higher percolation rate in Pajarito Canyon. Therefore, we simulate transport from the floor of Pajarito Canyon through the unsaturated zone to analyze the potential dose for this pathway, including three canyon percolation rates for the uncertainty analysis. The final step in the analysis of this pathway is to calculate the continued migration of the contaminants through the saturated zone, starting with the nuclide flux from the unsaturated zone.

The simulated aquifer-related dose resulting from lateral transport to the mesa sides is expected to be orders of magnitude higher than the true dose that might occur from this pathway for two reasons. First, the simulated lateral transport of the nuclides occurs because of the very low, fixed saturation boundary condition along the mesa sides. This causes a strong lateral pressure gradient that pulls water and subsequently nuclides from the mesa interior toward the sides. However, if drying really occurs throughout the mesa top in fractures and along surge beds rather than only at the mesa exterior, the resulting pressure gradient would decrease, leading to less contaminant movement toward the mesa sides.

Second, the flux is calculated as though the nuclides are immediately available for subsurface transport through the canyon bottoms once they reach the mesa edge, perhaps via surface runoff. However, because nuclides are heavy and nonvolatile, they actually would accumulate along evaporation sites rather than exiting the soil. Longmire et al. (1996) have observed elevated chloride, sulfate, and sodium concentrations in pore waters extracted from unsaturated-zone Bandelier tuff samples which suggest that evaporation leads to the concentration of dissolved species. Newman's (1996) data showing elevated chloride and stable isotope concentrations also support this discussion.

SATURATED-ZONE TRANSPORT

With the unsaturated-zone nuclide flux as the saturated-zone source term, advective-dispersive-reactive transport is simulated to locations downstream of the site boundary. Figure 10 shows concentration profiles at two locations in the saturated zone for the 1988-1995 ^{129}I inventory. The locations represent the point of maximum dose for the 1988-1995 waste and the 100-m downstream compliance point, which is 100 m downstream from the site fence line, but approximately 800 m from the 1988-1995 pits (Fig. 3). Such concentration information, along with analogous information for the other waste classes and the other two nuclides, is used in the formal dose assessment (Shuman, 1997b). The two curves have the same shape with dilution and mixing decreasing concentration by a factor of about three at the 100-m distance. Dilution at the 100-m compliance point increases with distance from the original waste site (i.e. aquifer dilution for the 1996-2044 waste is greater at the 100-m compliance point than for the 1957-1970 waste). The concentration profiles also mimic the unsaturated-zone contaminant flux curve shown in Figure 8. Using the current estimated dispersion coefficients, aquifer dilution of unsaturated-zone concentrations is approximately a factor of 500 between the maximum unsaturated-zone concentration and the aquifer concentration at the 100-m compliance point. The simulated plumes disperse throughout the 100-m depth of the model soon after entering the aquifer based on the chosen transport parameters. Therefore, concentration profiles at the 100-m compliance point are nearly uniform with depth with the highest concentration at the water table. This high dilution factor is evaluated later in the uncertainty analysis.

Dose Assessment

The dose conversion factors shown in Table 4 are applied to the three-dimensional ^{14}C, ^{129}I, and ^{99}Tc saturated-zone concentration fields to obtain dose fields. These dose fields are then summed to obtain the total groundwater dose and the groundwater component of the all-pathways dose for the entire PA inventory (1988-1995 plus 1996-2044 waste) and the Composite Analysis Inventory (all wastes). The 100-m compliance points can then be identified as the locations of maximum dose at distances 100 m from the site fenceline for various combinations of waste classes.

The DOE performance objectives are compared to the calculated maximum dose values in Table 5 for nuclides that have traveled continuously downward through the unsaturated zone. The comparison is shown for the base-case flow field, the highest-flow field, and the lowest-flow field at 1,000 years. Also compared are the peak doses during the 10,000-year uncertainty period for the base case. All doses calculated for this pathway are six or more orders of magnitude lower than the performance objectives. For the lowest-flow case, doses are negligible because over 99% of the inventory remains in the unsaturated zone.

The full dose assessment for the site is presented by Shuman (1997b). Shuman calculated a higher dose during the first 1,000 years for waste transported laterally to the mesa side than for waste that follows the continuous downward path to the water table. The earlier arrival time and higher aquifer concentrations for the lateral pathway are caused by the assumption of immediate release into Pajarito Canyon and the fast canyon recharge rate. For example, the peak aquifer dose for the base-case, unsaturated-zone flow field caused by migration toward the mesa side and subsequent deposition into Pajarito Canyon occurs after 800 years. The PA groundwater dose is 4.5×10^{-5} and the PA all-pathways dose is 1.3×10^{-4}. These doses are higher than those reported in Table 5, but still five to six orders of magnitude lower than the performance objectives.

The simulated lateral pathway is thought to be overestimated for reasons discussed previously. To calculate the impact of overestimating this pathway, a mass balance comparison of the downward and lateral pathways was performed. Over 10,000 years, approximately 30% of the mass exits laterally compared to that traveling downward. If this mass traveled downward, we would predict roughly a 30% increase in dose for the downward pathway, which is insignificant to the dose assessment (see Table 5).

UNCERTAINTY

As in any predictions of the long-term migration of solutes through the subsurface, the results of these transport simulations contain intrinsic uncertainty. Here we summarize what we believe are the more important uncertainties and discuss their impact. The greatest uncertainties associated with predicting aquifer-related doses from the site are related to our understanding of the mechanisms that control flow and transport within the unsaturated zone and our ability to model these mechanisms. At this point, we feel that uncertainty related to the hydrologic processes themselves (conceptual model uncertainty) dominates our ability to make accurate predictions of transport at the site more so than uncertainty related to the hydrologic and geochemical properties (data uncertainty). However, predicted doses using parameters from the most conservative ends of the uncertain ranges are still well below those that would cause concern.

UNSATURATED-ZONE FLOW

Insitu saturation data are difficult to match with any single infiltration rate using our current unsaturated-zone model. It is possible that the mesa and the submesa units are not strongly connected hydrologic systems. Higher saturations beneath the mesa may result from a recharge source other than percolation through the mesa or could represent moisture from a past, wetter climate. Evaporation is clearly an important mechanism controlling mid-mesa flux rates, yet it is only indirectly incorporated into the flow modeling through the application of low infiltration rates of one to ten mm/yr. By directly simulating evaporation in fractures and surge beds within the mesa interior, calculated solute migration through the mesa may behave similarly to that seen with environmental tracers such as chloride. These tracers accumulate within the mesa and have estimated travel times on the order of 1,000 to 17,000 years through the Bandelier Tuff (Newman, 1996). Accumulation of nuclides within the mesa top would lead to a reduction in predicted doses.

The mesa-top infiltration rate is the strongest control on the simulated migration of waste through the unsaturated zone. It controls both the source release rate and subsequent downward solute migration. We bounded this uncertainty by considering a base-case flow field and high- and low-flow cases. As shown in Table 5, a variation in mesa-top infiltration rate from 1 mm/yr to 10 mm/yr results in a range of six orders of magnitude in the 1000-year groundwater-related doses. Clearly a good understanding of this key parameter is important to the dose assessment. However, because doses are so much less than the performance objectives, conservative yet realistic infiltration rates seem adequate for this site.

Other uncertainties are related to flow within the deeper unsaturated-zone units for which little hydrologic data are available. The simulations take virtually no credit for transport times through the Cerros del Rio Basalts, which make up more than 50% of the unsaturated zone. Understanding the mechanisms that govern flow and transport in the deeper unsaturated-zone and incorporating them into the model could add hundreds if not thousands of years to predicted transport times and result in lower peak aquifer concentrations.

The transport results are based on the steady-flow assumption and on the use of matrix hydrologic properties for all but the basalts at the site. Our understanding of the response of this fractured system to transient flow events remains uncertain. Transient calculations (Birdsell et al., 1997) indicate that the steady flow assumption is adequate because fluctuations in both saturation and contaminant flux rates dampen with depth even when including fractures in the upper two units. Fracture infiltration studies (Soll and Birdsell, 1997) led us to the conclusion that fracture flow is difficult to initiate and short lived in the upper two tuff units at the observed low field saturations. This conclusion helps justify the use of the matrix hydrologic properties for the calculations. We should note that only the upper two tuff units are considered to have significant fracturing (Krier et al., 1997), and that the uppermost unit is excavated during disposal operations. The waste travels

through only one highly fractured unit (Unit 1v-u) above the basalts and even if fracture flow dominates there, the underlying matrix units will attenuate transient pulses. Although we are confident in the assumptions made here, verifying the absence of young environmental isotopes such as bomb-pulse ^{36}Cl at depth would add support to these assumptions.

Although there is variability in hydrologic properties at the site, mean values were chosen for the properties used in the modeling. A sensitivity analysis using the minimum and maximum reported saturated hydraulic conductivity values for the tuff units (Birdsell et al., 1997) showed variations in unsaturated-zone travel times of approximately ±25% from the mean. With higher conductivity values, the flux-versus-time curves shown in Figure 8 move to the left, and predicted doses increase. This shift could potentially elevate doses by about two orders of magnitude, still well below the performance objectives. Heterogeneity in hydrologic properties could lead to preferential flow paths through the unsaturated zone that could produce shorter travel times and regions of higher flux. The effects of heterogeneity are discussed later.

SATURATED-ZONE FLOW

The saturated zone is modeled as a homogeneous and isotropic medium, while the true system is heterogeneous. Heterogeneity can lead to preferential flow paths that may yield higher aquifer concentrations. Aquifer concentrations are, however, limited by the flux of nuclides through the unsaturated zone and even the maximum calculated aquifer doses, before any migration in the aquifer, are six orders of magnitude less than acceptable limits.

The aquifer velocity may be double that used here (Purtymun 1995), which would move the plume more quickly toward the compliance point and possibly dilute the plume. This effect is small because the travel time through the aquifer is short compared to that through the unsaturated zone. One other uncertainty is related to the modeled aquifer depth. The plume disperses throughout the entire modeled depth of 100 meters. Had the depth been increased, the plume would have dispersed even further with a corresponding decrease in concentration.

TRANSPORT PROPERTIES

The transport simulations are very sensitive to the value of the distribution coefficient, Kd, in the unsaturated zone. Uncertainty in this parameter for weakly sorbing nuclides plays an important role in the results of this analysis. According to our simulations, a nuclide with a Kd greater than 2.5 will not reach the saturated zone within 10,000 years. Previous simulations (Birdsell et al., 1995) indicate that a Kd as low at 0.3 will retard nuclides sufficiently to prevent breakthrough to the aquifer within 1000 years. Site-specific values for several nuclides with large inventories or expected low distribution coefficients were measured to decrease the uncertainty in the predictions that results from data uncertainty for this parameter (Longmire et al., 1996). The combination of a

low-Kd nuclide traveling along a fast flow path could lead to breakthrough of nuclides other than the three nonsorbing species found to be of concern. However, for this mechanism to be significant to the dose assessment, fast flow paths would need to contact a significant portion of the inventory.

In the saturated-zone model, longitudinal and transverse dispersivity values of 20 m and 2 m are used. Larger dispersivity values are justifiable based on the distance of the pits to the 100-m compliance point. For example, the 1996-2044 pits are on the order of 1,300 m from the compliance point, which leads to longitudinal and transverse dispersivity values of 130 m and 13 m respectively based on Neuman's (1990) empirical fit to field data. Longitudinal and transverse dispersivity values of 1 m and 0.1 m are used for the unsaturated-zone modeling, and again higher values may be warranted. The effect of increasing the dispersivity in either case is that an increased longitudinal dispersivity results in a faster arrival time for the plume's leading edge but a lower peak concentration. An increase in the transverse dispersivity also leads to a lower peak concentration. If higher longitudinal dispersivity values were used, the maximum dose for the 1,000-year compliance period would increase, while the maximum dose for the 10,000-year uncertainty period would decrease. Doses would not increase above the maximum doses during the uncertainty period (Table 5), and therefore would not approach the performance objective. If we assumed negligible dispersion by using lower dispersivity values, the arrival of the plume's leading edge would be delayed but peak concentrations would be higher resulting in lower doses during the 1000-year compliance period, but higher doses during the 10,000-year uncertainty period.

DISCUSSION and CONCLUSIONS

Numerical simulations are used to predict the long-term migration of radionuclides for the performance assessment of a low-level radioactive waste disposal facility. This example describes a method for using detailed process-based models rather than higher-level performance assessment models to perform the ground water transport calculations required for a site performance assessment. The method first requires some knowledge of the site geology, hydrology, and geochemistry, which is used to define the conceptual model of the flow and transport processes that occur at the site. The conceptual model is then described numerically using processed-based numerical models that simulate groundwater flow, radionuclide transport, and dose. The predictions simulate source releases followed by subsequent transport through the unsaturated and saturated zones. The domains are simulated separately but linked through the application of the unsaturated-zone contaminant flux as a boundary condition to the saturated-zone model. A range of unsaturated-zone flow rates is simulated in order to address the effect of uncertainty in infiltration rate on aquifer concentrations. This process-based method is applicable to other low-

level waste sites and may provide a more science-based, defensible argument for the acceptance of a PA than a more traditional performance assessment model.

Screening and scaling techniques as well as simplifying assumptions can be used to make a full site assessment tractable. The screening and scaling techniques listed below (Items 1 through 3) are applicable to any site. The simplifying assumptions (Items 4 and 5) are site specific but illustrate the use of scoping calculations to define the importance of including processes and/or analyses in the study.

1) Calculations for the LANL site show only the three nonsorbing nuclides ^{14}C, ^{129}I, and ^{99}Tc reaching the aquifer during the 1,000-year compliance period or the 10,000-year uncertainty period. Therefore, no formal transport calculations are required for the remaining nuclides in the inventory. With this simple screening technique, the compliance period is compared to the travel times for nuclides with increasing sorption coefficients. Once a cut-off Kd value is found, nuclides with larger Kd values need not be considered.

2) For longer or unspecified compliance periods a more general screening technique is applied. Generic breakthrough curves are used to estimate travel time as a function of Kd. Then each radionuclide's half-life is compared to its predicted travel time. If several half-lives (twenty is very conservative) are less than the travel time, the nuclide will decay sufficiently so that no release is predicted and an assessment for that species is not necessary. Daughter products must also be considered.

3) The spatial variability of the source term is important for the example presented in this paper. At other sites, spatial source term information may be unavailable or unimportant. For such sites, generic breakthrough curves developed for the screening can be scaled (with a correction for radioactive decay) based on the inventory of any nuclides still requiring full assessment.

4) Although the site conceptual model shows that transients and fracture flow may affect transport at the site, a steady-flow, matrix-dominated, unsaturated-zone model is used. Smaller-scale simulations, which indicate that transients are damped with depth (Birdsell et < biblio >) and that fracture flow in the upper units is difficult to maintain (< biblio >), justified the assumptions.

5) A formal uncertainty analysis is not necessary for this case study because simulated doses are several orders of magnitude lower than performance measures, and the informal arguments concerning the uncertainty of the simulations indicate

that the site will remain in compliance even if these factors are taken into account. A formal uncertainty analysis may only be required if predicted doses approach regulatory limits.

Process-based predictions not only provide a more science-based site assessment; they can also highlight data needs or point out data that is not crucial to the performance assessment. For this example, the mesa-top infiltration rate is the strongest control over the predicted dose. Chloride profiles (Newman, 1996) and predicted saturation profiles indicate that the range of infiltration rates we have chosen are conservative for the site. However, we are unable to match field data with the steady-flow, uniform infiltration, unsaturated-zone model. If infiltration is spatially variable or is transient, the site's performance could be less robust than indicated by our study. For this reason, a continued effort that couples chloride and isotope analyses with modeling studies is planned to better understand local and site-wide net infiltration.

In contrast, although we have little knowledge of the hydrologic properties of the basalt unit at the site, we feel that such data are not currently required. The site appears to perform significantly better than is required despite our assumption of nearly instantaneous transport through the basalt unit. Any data gathered to increase our understanding of transport through the basalt would increase travel times and decrease predicted aquifer concentrations.

REFERENCES

Birdsell, K.H., W.E. Soll, K.M. Bower, A.V. Wolfsberg, T. Orr, T.A. Cherry, (1997). "Simulations of Groundwater Flow and Radionuclide Transport in the Vadose and Saturated Zones Beneath Area G, Los Alamos National Laboratory," Los Alamos National Laboratory manuscript LA-13299-MS.

Birdsell, K.H., W.E. Soll, N.D. Rosenberg, and B.A. Robinson, (1995). "Numerical Modeling of Unsaturated Groundwater Flow and Radionuclide Transport at MDA G," Los Alamos National Laboratory document LA-UR-95-2735.

Bishop, C.W., (1991). "Hydrologic Properties of Vesicular Basalt," Masters thesis, University of Arizona.

Bowen, B.M., (1990). "Los Alamos Climatology," Los Alamos National Laboratory Manuscript LA-MS-11735.

Conca, J.L., and J. Wright, (1992). "Diffusion and Flow in Gravel, Soil, and Whole Rock," *Applied Hydrogeology*, Vol 1, No. 1, pp. 5-24.

Degueldre, C., I. Triay, J. Kim, P. Vilks, M. Laaksoharju, and N. Mielkeley (1997). "Groundwater Colloid Properties: A Global Approach, *Environmental Science and Technology* (Submitted).

Fisher, R.V. (1979) "Models for pyroclastic surges and pyroclastic flows," *Journal of Volcanology and Geothermal Research* **6**, 305-318.

Gable, C.W., T. Cherry, H. Trease, and G.A. Zyvoloski, (1995). "GEOMESH Grid Generation," Los Alamos National Laboratory document LA-UR-95-4143.

Gelhar, L.W., C. Welty, K.T. Rehfeldt, (1992). "A Critical Review of Data on Field Scale Dispersion in Aquifers," *Water Resource Research* **28**, 1955-1974.

Hollis, D., E. Vold, R. Shuman, K. Birdsell, K. Bower, W. Hansen, D. Krier, P. Longmire, B. Newman, D. Rogers, and E. Springer, (1997). "Performance Assessment and Composite Analysis for the Los Alamos National Laboratory Disposal Area G," Los Alamos National Laboratory document LA-UR-97-85, Report-54G-013.

Jury, W.A., W.R. Gardner, and W.H. Gardner, (1991). *Soil Physics*, J. Wiley & Sons, Inc.

Kersting, A.B., D.W. Effurd, D.L. Finnegan, D.J. Rokop, D.K.Smith, and J.L. Thompson, (1999). "Migration of Plutonium in Groundwater at the Nevada Test Site," *Nature* **397**, 56-59.

Klavetter, E.A., and R.R. Peters, (1986). "Estimation of Hydrologic Properties of an Unsaturated Fractured Rock Mass," Sandia National Laboratory report SAND84-2642.

Krier, D., P. Longmire, R.H. Gilkeson, and H.J. Turin, (1997). "Geologic, Geohydrologic and Geochemical Data Summary of MDA G, TA-54 Los Alamos National Laboratory," Los Alamos National Laboratory document LA-UR-95-2696.

Longmire, P., C.R. Cotter, I.R. Triay, J.J. Kitten, C. Hall, J. Bentley, D. Hollis, and A.I. Adams, (1996). "Batch Sorption Results for Americium, Neptunium, Plutonium, Technetium, and Uranium Transport through the Bandelier Tuff, Los Alamos, New Mexico," Los Alamos National Laboratory document LA-UR-96-4716.

Neuman, S.P., (1990). "Universal Scaling of Hydraulic Conductivities and Dispersivities in Geological Media", *Water Resources Research* **26**, 1749-1758.

Newman, B.D., (1996). "Vadose Zone Water Movement at Area G, Los Alamos National Laboratory, TA-54: Interpretations Based on Chloride and Stable Isotope Profiles," Los Alamos National Laboratory document LA-UR-96-4682.

Purtymun, W.D., (1995). "Geologic and Hydrologic Records of Observation Wells, Test Holes, Test Wells, Supply Wells, Springs, and Surface Water Stations in the Los Alamos Area," Los Alamos National Laboratory manuscript LA-12883-MS.

Purtymun, W.D., (1984). Hydrologic Characteristics of the Main Aquifer in the Los Alamos Area: Development of Groundwater Supplies," Los Alamos National Laboratory manuscript LA-9957-MS.

Rogers, D.B., and B.M. Gallaher, (1995). "The Unsaturated Hydraulic Characteristics of the Bandelier Tuff," Los Alamos National Laboratory manuscript LA-12968-MS.

Rogers, D.B., P. Longmire, B.D. Newman, K.H. Birdsell, W.E. Soll, and E.L. Vold, (1997). "Conceptual Model for Subsurface Transport at MDA G," Los Alamos National Laboratory report LA-UR-97-179.

Shuman, R., (1997a). "Radioactive Waste Inventory for the TA-54, Area G Performance Assessment and Composite Analysis," Rogers and Associates Engineering Corp. report, RAE-9629/91B-2.

Shuman, R., (1997b). "Radiological Dose Assessment for the TA-54, Area G Performance Assessment and Composite Analysis," Rogers and Associates Engineering Corp. report, RAE-9629/91B-1.

Soll, W.E. and K. H. Birdsell, (1998). "Influence of Coatings and Fills on Flow in Fractured, Unsaturated Tuff Porous Media Systems," *Water Resources Research* **34**, 193-202.

Turin, H. J., (1995). "Subsurface Transport Beneath MDA G: A Conceptual Model," Los Alamos National Laboratory document LA-UR 95-1663.

van Genuchten, M.T., (1980). "A Closed-Form Equation for Predicting the Hydraulic Conductivity of Unsaturated Soils," *Soil Science Society of America Journal* **44**, 892-898.

Vaniman, D., G. Cole, J. Gardner, J. Conaway, D. Broxton, S. Reneau, M. Rice, G. WoldeGabriel, J. Blossom, and F. Goff, (1996). "Development of a Site-Wide Geologic Model for Los Alamos National Laboratory," Los Alamos National Laboratory unpublished document.

Vold, E.L., D. Hollis, P. Longmire, E. Springer, K. Birdsell, and R. Shuman, (1996). "The Role of a Detailed Aqueous Phase Source Release Model in the LANL Area G Performance Assessment," Los Alamos National Laboratory document LA-UR-96-368.

Vold, E.L., (1996). "Analysis of Liquid Phase Transport in the Unsaturated Zone at a Mesa Top Disposal Facility," Los Alamos National Laboratory document LA-UR-96-370.

Vold, E.L. and R. Shuman, (1996). "Phase Two of the Source Release Modeling for the Los Alamos Area G Disposal Facility Performance Assessment," Los Alamos National Laboratory report LA-UR-96-4786.

Wilson, M., J. Gauthier, R. Barnard, G. Barr, H. Dockery, E. Dunn, R. Eaton, D. Guerin, N. Lu, M. Martinez, R. Nilson, C. Rautman, T. Robey, B. Ross, E. Ryder, A. Schenker, S. Shannon, L. Skinner, W. Halsey, J. Gansemer, L. Lewis, A. Lamont, I. Triay, A. Meijer, and D. Morris (1994). "Total-System Performance Assessment for Yucca Mountain - SNL Second Iteration (TSPA-1993)", Sandia National Laboratory report SAND93-2675.

Zyvoloski, G.A., B.A. Robinson, Z.V. Dash, and L.L. Trease, (1997). " Summary of the Models and Methods for the FEHM Application – A Finite Element Heat- and Mass-Transfer Code," Los Alamos National Laboratory manuscript LA-13307-MS.

Table 1. Hydrologic Properties			
Unit	**Ksat (cm/s)**	**porosity**	**van Genuchten θ_r, α (cm^{-1}), n**
Pit (Crushed Unit 2 Tuff)[b]	25.0	0.479	0.00767, 0.00663, 2.00389
Unit 2[a]	4.27×10^{-4}	0.481	0.013, 0.0060, 1.890
Unit 1v-u[a]	1.48×10^{-4}	0.517	0.002, 0.0030, 1.932
Unit 1v-c[a]	1.67×10^{-4}	0.509	0.009 0.0033,1.647
Unit 1g[a]	1.88×10^{-4}	0.480	0.006, 0.0053, 1.745
Cerro Toledo[a]	8.65×10^{-4}	0.473	0.008, 0.0152, 1.506
Otowi Member[a]	2.49×10^{-4}	0.435	0.0188, 0.0059, 1.713
Guaje Pumice[b]	1.5×10^{-4}	0.667	0.0, 0.00081, 4.0264
Puye Formation[d,e]	4.6×10^{-3}	0.25	0.045, 0.145, 2.68
Cerros del Rio basalts[c] *(matrix only)*	9.7×10^{-5}	0.228	0.015, 0.0384, 1.474
Cerros del Rio basalts[c] (fracture properties) *(equivalent continuum)*	9.7×10^{-5} 9.7×10^{2}	1×10^{-4} 1×10^{-4}	6.6×10^{-6}, 0.0384, 1.474 3.0×10^{-6}, 0.0384, 1.474

[a]Mean values from Krier et. al, 1997, [b]E. Springer (personal communication), [c]Bishop (1991), [d]Purtymun (1984), [e]Carsel and Parrish (1988).

Table 2. Median Distribution Coefficients (Kd (ml/g) for Nuclides on Intact and Crushed, Unsaturated Bandelier Tuff and on Saturated Samples			
	Intact Tuff	**Crushed Tuff**	**Aquifer**
Nonsorbing Nuclides			
^{14}C, ^{129}I, ^{99}Tc	0	0	0
Weakly Sorbing Nuclides			
^{237}Np	2.25	7.5	0.151
^{233}U, ^{234}U, ^{235}U, ^{236}U, ^{238}U	2.43	2.61	4.85
^{93}Mo	4	4	4
^{238}Pu, ^{239}Pu, ^{240}Pu, ^{241}Pu, ^{242}Pu	4.13	711	13.95
Strongly Sorbing Nuclides			
^{40}K	15	15	15
^{210}Pb	25	25	25
^{32}Si	35	35	35
^{244}Cm, ^{152}Eu, ^{154}Eu, ^{148}Gd, ^{231}Pa, ^{147}Sm, ^{151}Sm	50	50	50
^{113}Cd-m	80	80	80
^{108}Ag-m	90	90	90
^{93}Nb-m, ^{94}Nb	100	100	100
^{90}Sr	116	116	116
^{227}Ac, ^{249}Cf, ^{252}Cf	130	130	130
^{226}Ra, ^{228}Ra	200	200	200
^{137}Cs	428	428	428
^{182}Hf, ^{229}Th, ^{230}Th, ^{232}Th, ^{44}Ti	500	500	500
^{133}Ba	946	946	946
^{241}Am, ^{243}Am	2359	2050	141

Table 3. Infiltration rates (mm/yr) used as upper boundary conditions.			
	Mesa Top	**Cañada del Buey**	**Pajarito Canyon**
1_1_20 (Lowest Flow Case)	1	1	20
5_1_20	5	1	20
5_1_50 (Base Case)	5	1	50
10_1_20	10	1	20
10_5_100 (Highest Flow Case)	10	5	100

Table 4. Factors for converting aquifer concentration to dose.			
Nuclide	**Conversion from moles/liter to Ci/m^3**	**Conversion from Ci/m^3 to mrem/yr for the drinking water pathway dose**	**Conversion from Ci/m^3 to mrem/yr for the all pathways dose**
^{14}C	6.24×10^{4}	1.53×10^{6}	4.11×10^{6}
^{99}Tc	1.686×10^{3}	9.49×10^{5}	3.04×10^{6}
^{129}I	21.03	2.04×10^{8}	2.70×10^{8}

Table 5. Maximum groundwater and all-pathways doses for the PA and CA wastes (mrem/yr).			
	PA - Ground Water	**PA - All Pathways**	**CA - All Pathways**
Performance Objective	4	25	100
1,000 yr (Base Case)	2.4×10^{-7}	6.5×10^{-7}	3.7×10^{-5}
Peak Dose (Base Case)	3×10^{-5} @ ~4500 yrs	1×10^{-4} @ ~4500 yrs	2×10^{-3} @ ~3000 yrs
1,000 yr (Highest Flow)	8.0×10^{-6}	2.2×10^{-5}	1.4×10^{-3}
1,000 yr (Lowest Flow)	9×10^{-12}	2×10^{-11}	1×10^{-10}

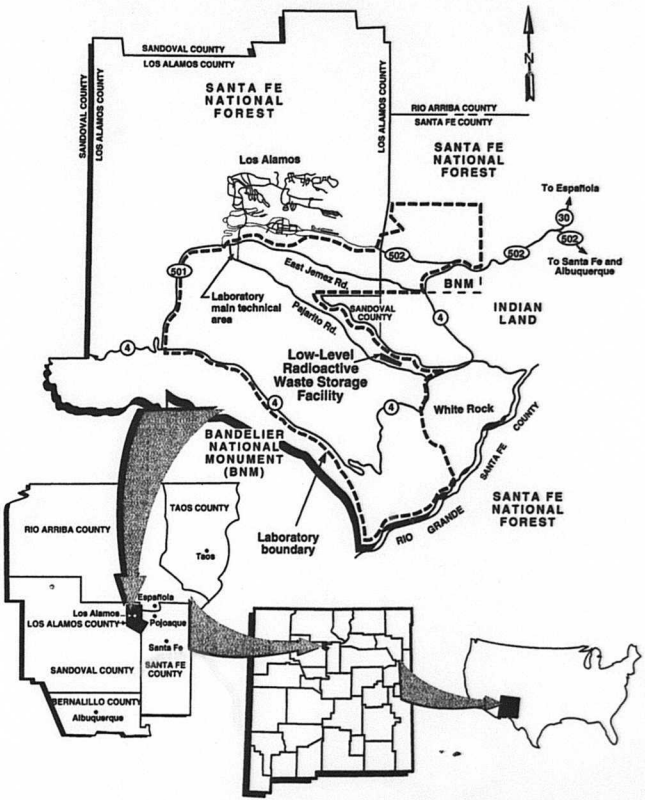

Figure 1. Location of the low-level waste site at Los Alamos National Laboratory.

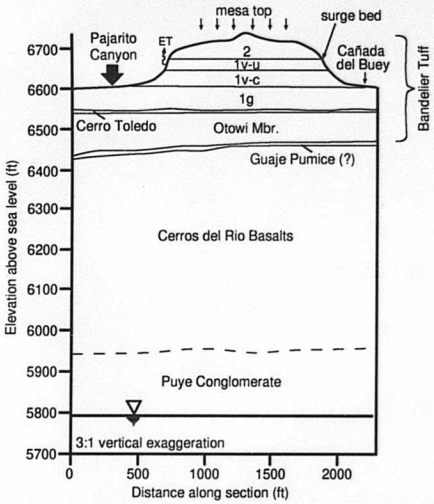

Figure 2. Two-dimensional stratigraphy (Krier et al., 1997) with boundary conditions for the unsaturated-zone simulations. The upper six units make up the Bandelier Tuff.

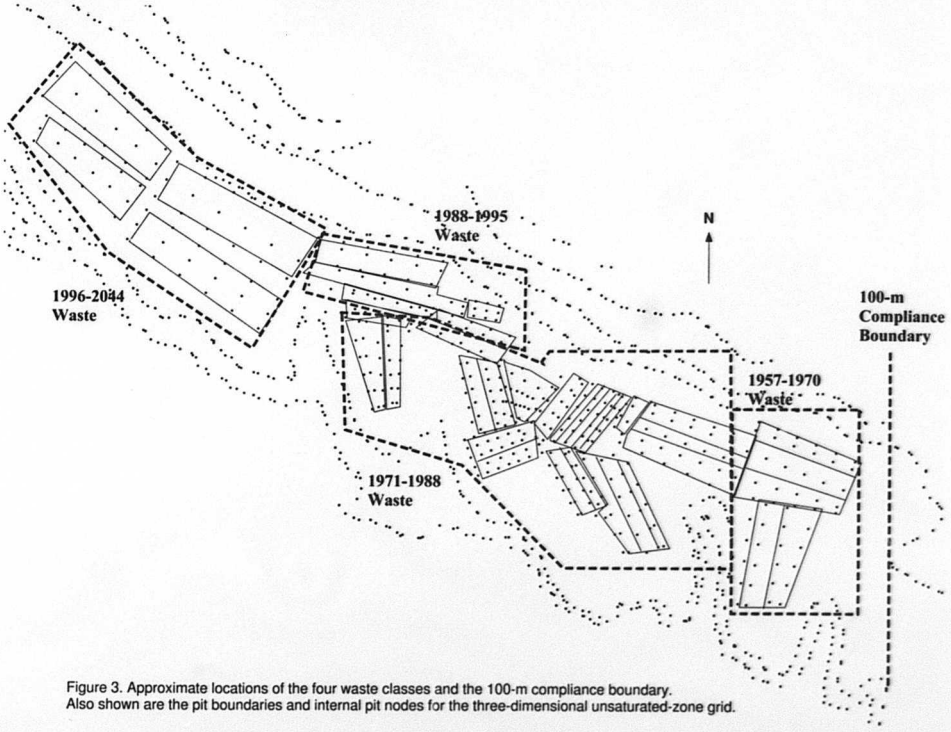

Figure 3. Approximate locations of the four waste classes and the 100-m compliance boundary.
Also shown are the pit boundaries and internal pit nodes for the three-dimensional unsaturated-zone grid.

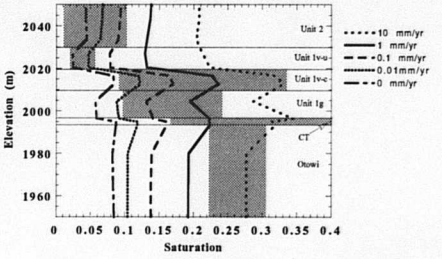

Figure 4. Comparison of site data (gray boxes) to calculated steady-state saturation profiles for several infiltration rates. Calculated profiles are located at the center of the cross section.

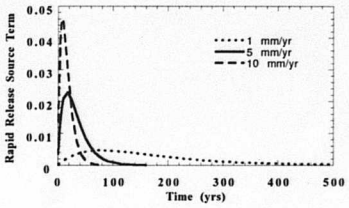

Figure 5. The dependence of the rapid-release, source term model on the infiltration rate.

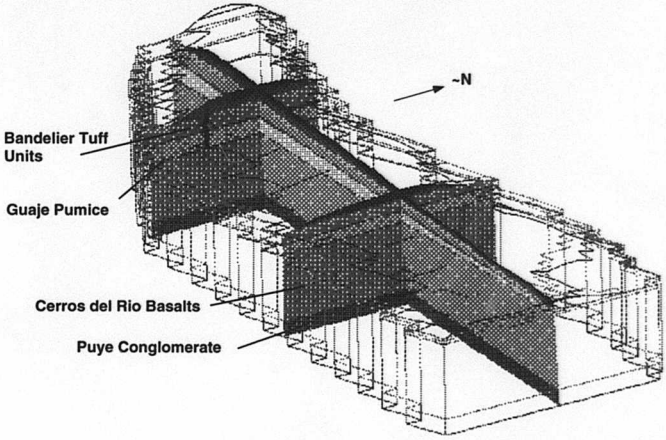

Figure 6. Three-dimensional stratigraphic framework model of the site.

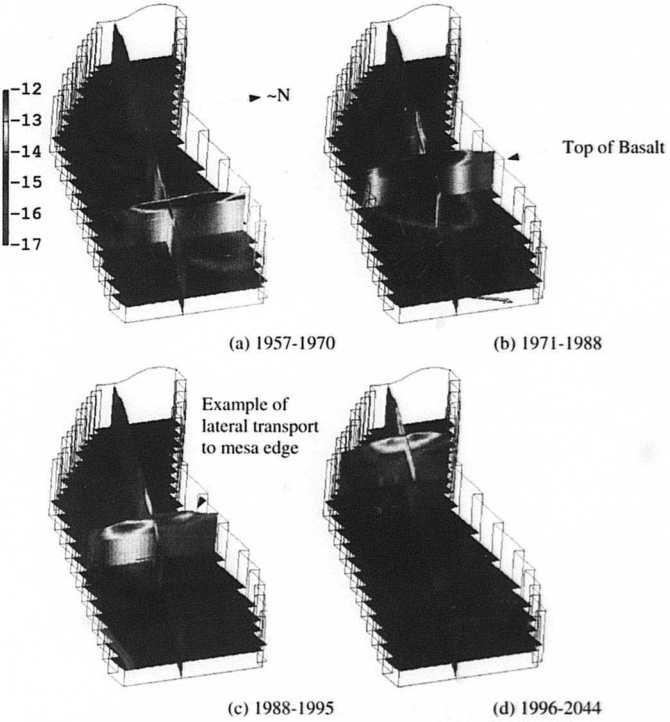

Figure 7. 129I plumes (log concentration, moles/liter) in the unsaturated zone at 1000 years for the four different source regions, base-case flow field.

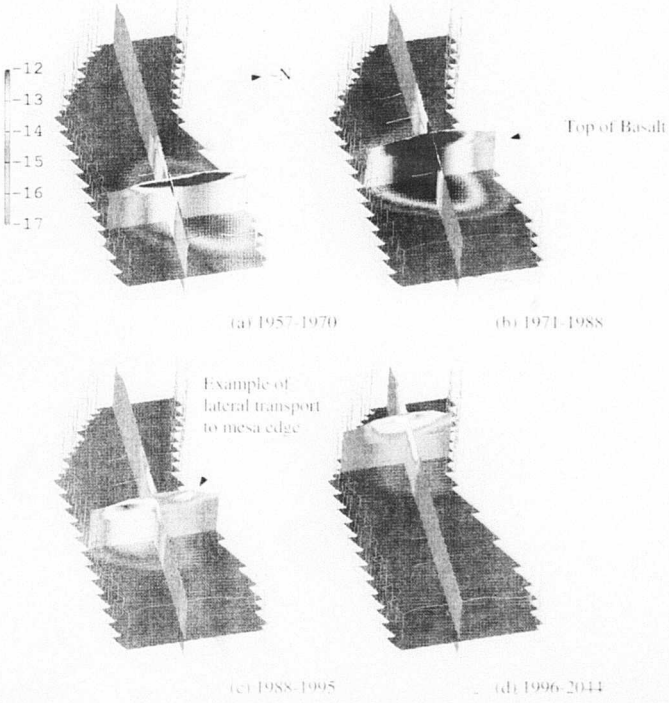

Figure 7. 129I plumes (log concentration, moles/liter) in the unsaturated zone at 1000 years for the four different source regions, base-case flow field.

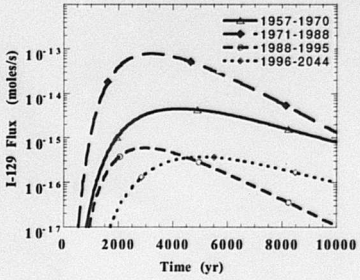

Figure 8. Total flux of ^{129}I from the unsaturated zone to the saturated zone from the four source regions, base-case flow field (5_1_50).

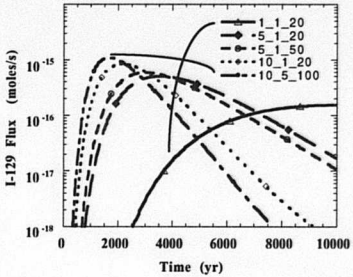

Figure 9. Total flux of the historical ^{129}I inventory from the unsaturated zone to the saturated zone for various flow cases.

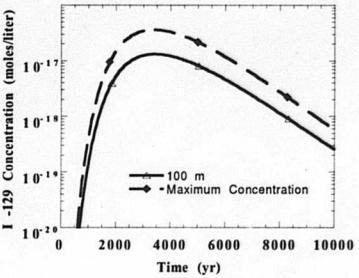

Figure 10. Concentrations in the saturated zone for the ^{129}I Historic inventory at the point of maximum concentration and at the 100-m compliance point with the base-case, unsaturated-zone flow field.